Coupled hydro-mechanical behaviour of a Kaolin Clay in the context of the geothermal use of geotechnical structures

Timon Kayser[1*], *Wiebke* Baille[1], *Merita* Tafili[1], *Torsten* Wichtmann[1]

[1]Chair of Soil Mechanics, Foundation Engineering and Environmental Geotechnics, Ruhr-University Bochum, Germany

Abstract. An experimental study regarding the hydro-mechanical behaviour of a Malaysian Kaolin is presented. Strain rate-controlled oedometer tests have been conducted on compacted samples. The influence of initial water content on the pore-size distribution (PSD) of compacted samples was investigated by Mercury Intrusion Porosimetry (MIP) tests. The drying path of the soil-water characteristic curve was experimentally determined for initially compacted samples and slurry samples. The preconsolidation stress was found to increase with increase in initial dry density and with decrease in initial water content. The compression curves merge into a single line, as soon as they have reached full saturation during loading. Samples at the dry side of Proctor water content showed a bi-modal PSD, whereas a mono-modal PSD was found for Proctor water content and at the wet side. The different initial compaction states of the samples were getting reflected in the drying SWCC until a suction of about 2 MPa, beyond which the drying paths were found to be identical.

1 Introduction

In the context of the development of renewable energies, the geothermal use of geotechnical structures is becoming increasingly relevant. The most prominent example of such structures are energy piles. Energy piles now act as heat exchangers with the earth in addition to transferring building loads into the ground. The temperature imposed into the ground varies cyclically due to seasonal or daily changes in temperature. Furthermore, the soil surrounding the piles may be in a saturated or unsaturated state with varying degree of saturation and suction. Hence the soil around the energy piles is subjected to thermo-mechanical or thermo-hydro-mechanical loading. It is well known that the degree of saturation has an impact on the mechanical soil properties such as shear strength, which increases with increasing suction and decreasing degree of saturation [1]. However, the impact of cyclic THM-loading scenarios on saturated and unsaturated clay soil has not been studied in detail in literature so far. A current joint research project at Ruhr-University Bochum and Charles University Prague aims to investigate the cyclic THM-behaviour of a kaolin clay. In this paper, first experimental results by RUB obtained at standard temperature of 20 °C are presented.

For this purpose, a series of tests was carried out, involving basic geotechnical characterisation of the kaolin, strain-controlled oedometer tests covering two different stress ranges on samples with varying initial void ratios and gravimetric water content, determination of the drying soil-water-characteristic curve, and the pore-size distribution of specimens having different initial water contents at identical dry densities.

2 Material

The tests in this study were performed on Malaysian kaolin. The clay is comprised of 48% muscovite, 46% kaolinite, 5.5% quartz and 0.5% rutile [2].

The grain size distribution was determined by means of a sedimentation analysis [3]. The material is composed of 20% clay, 78% silt and 2% fine sand as depicted in Fig. 1.

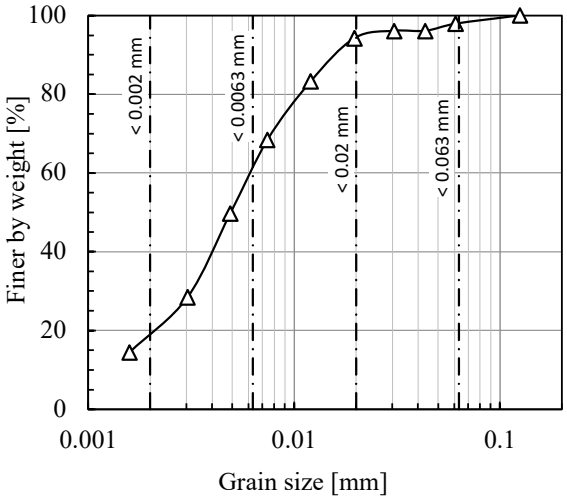

Fig. 1. Grain size distribution of Malaysian kaolin

The liquid limit was determined using the fall cone method [4] and it was found to be $w_L = 60\%$. The plastic limit of the material was found to be 34%, resulting in a plasticity index of 26% [4]. The Atterberg limits agreed well with former values determined by Duque et al.

* Corresponding author: timon.kayser@rub.de

2021 [5]. According to DIN 18196 [6] (see Fig. 2)., the soil is classified as a silt with high plasticity (MH). The grain density was found to be 2.70 g/cm³ [7].

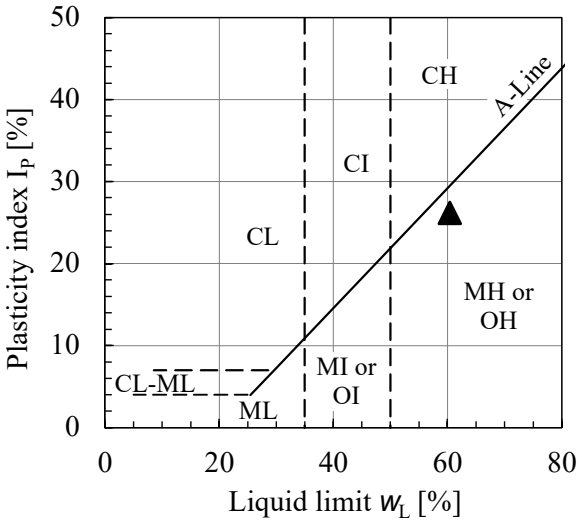

Fig. 2. Plasticity chart for Malaysian kaolin

By performing a standard Proctor test according to German standard DIN 18127 [8] (W ≈ 0.6 MNm/m³) the optimal water content was found to be w_{pr} = 32% with a Proctor density of ρ_{pr} = 1.35 g/cm³, corresponding to a void ratio of e = 1.00 (Fig. 3).

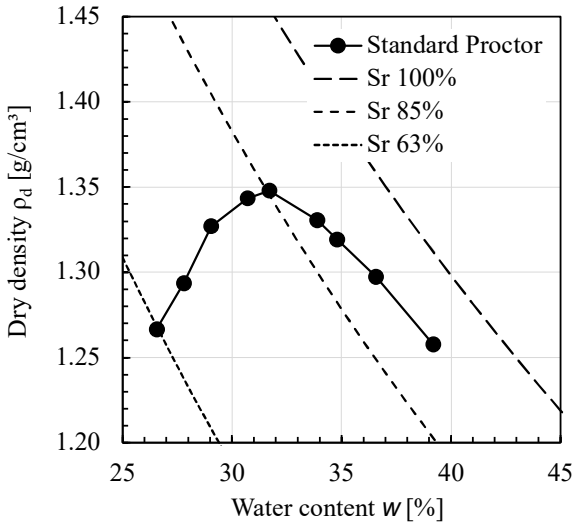

Fig. 3. Standard Proctor curve

3 Strain - controlled oedometer tests

In order to investigate the influence of the water content on the compression behaviour several strain rate-controlled oedometer tests with different initial water contents and dry densities were performed.

3.1 High Stress Oedometer tests with varying initial water content

The oedometric behaviour of compacted unsaturated Malaysian kaolin was determined by performing strain-rate-controlled oedometer tests in a high pressure oedometer [11]. The applied strain rate was $\dot{\varepsilon}_v$ = 0.1%/min and the resulting vertical stress during loading and unloading was measured. The three samples were compressed until a vertical stress of 10 MPa was reached, subsequently they were unloaded to 1 MPa and reloaded until maximum vertical stress of 25 MPa (Fig. 4). Prior to testing, the samples were statically compacted directly in the oedometer ring using a separate compaction device. Sample dimensions are 50 mm in diameter and 20 mm in height. The samples were compacted to a low target dry density of 1.10 g/cm³, corresponding to a target void ratio e of 1.45 at different water contents (w = 14.6%, w = 23.1%, w = 31.9%).

Tab. 1: Initial conditions and selected states during strain-controlled high pressure oedometer tests of Malaysian Kaolin

Sample	No. 1	No. 2	No. 3
$\rho_{d,0}$ [g/cm³]	1.10	1.12	1.10
w_0 [%]	14.6	23.1	31.9
e_0 [-]	1.45	1.41	1.45
S_{r0} [-]	0.27	0.44	0.59
$S_{r,final}$ [-] 1)	0.90	1.00	1.00
$S_{r,final}$ [-] 2)	1.00	1.00	1.00
e at S_r = 1 [-] 2)	0.39	0.62	0.86
σ_{pre} [kPa]	355	190	130
C_C [-] (S_r < 1) 2)	0.54	0.59	0.61
C_C [-] (S_r = 1) 2)	0.40	0.41	0.41
C_S [-] (1 to 10 MPa)	0.08	0.09	0.08

1) measured after dismantling the specimen
2) calculated based on initial conditions

The two smaller water content values (w = 14.6%, w = 23.1%) are on the dry side and the water content w = 31.9% corresponds to the optimum water content determined in the Proctor test (see Fig. 3 and Tab. 1).

The oedometric curves of the three samples are shown in Fig. 4.

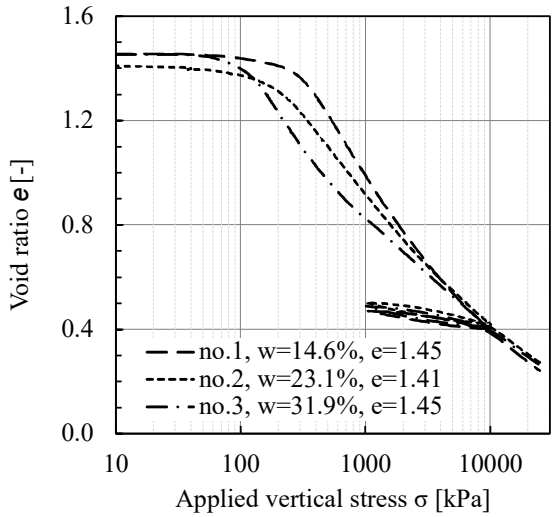

Fig. 4. Compression-decompression curves of samples no. 1, 2, and 3 at varying initial water content

During the loading paths, the gravimetric water content is assumed to remain constant until full saturation is reached. From the point of full saturation onwards the degree of saturation is assumed to be constant (S_r = 100%) and the corresponding water content is calculated. The measurement of final water content after dismantling confirmed the assumption.

The void ratio at which the samples reached full saturation due to compression was calculated based on known initial conditions and the measured sample deformation. The void ratio where full saturation was reached is 0.39, 0.62, and 0.86 for the samples no. 1, 2, and 3 with 14.6%, 23.1% and 31.9% initial water content, respectively. The corresponding vertical stresses were 9.50, 3.49, and 0.83 MPa. Beyond about 3.5 MPa, sample no. 2 and no. 3 both are saturated and merge; at about 9.5 MPa sample no. 1 has reached full saturation and merges with the saturated first loading paths of samples no. 2 and 3. At stresses smaller than about 2 MPa, sample no. 3 compacted at the Proctor water content (w = 31.9%) shows smallest resistance to compression, which is consistent with its higher initial degree of saturation, thus, smaller initial suction, as compared to the samples at dry side of optimum water content (sample no. 1 and 2). The above statements are supported by the compression index values of the three samples determined for the various stress ranges. The compression index C_C of sample no. 1 (w = 14.6%) equals 0.54. Samples no. 2 (w = 23.1%) and no. 3 (w = 31.9%) have compression indices of 0.59 and 0.61, respectively. After being fully saturated at stresses beyond about 3.5 MPa, the compression indices of the samples are nearly identical (0.40 and 0.41).

The preconsolidation stress σ_{pre} can be estimated by identifying the transition between the elastic and plastic zone during first loading according to Casagrande's graphical method. The preconsolidation stress for samples no. 1 (w = 14.6%) was about 355 kPa, for sample no. 2 (w = 23.1%) 190 kPa, and for sample no. 3 (w = 31.9%) it was approximately 130 kPa. The results are in accordance to literature, showing higher values of preconsolidation stress for samples with smaller initial water content and degree of saturation, thus, higher suction.

The unloading-reloading paths of the three samples were found to be very similar, since at beginning of unloading at 10 MPa, all three samples showed full saturation and nearly identical void ratios. The respective swelling indices C_S were 0.08, 0.09, and 0.08 for sample no. 1 (w = 14.6%), sample no. 2 (w = 23.1%), and sample no. 3 (w = 31.9%), respectively.

The results presented in Fig. 4 will be further used to determine the needed compaction stress at any target void ratio. For example, the static compaction stress needed to reach Proctor density of 1.35 g/cm^3, corresponding to a void ratio of 1.00, equals 440 kPa for sample no. 3 (w = 31.9%), 720 kPa for sample no. 2 (w = 23.1%) and 970 kPa for sample no 1 (w = 14.6%).

3.2 Oedometer tests with varying initial dry density

In the second test series, strain rate-controlled oedometer tests ($\dot{\varepsilon}_v$ = 0.1%/min) were performed on samples with varying initial void ratios at similar water content over a stress range up to 2 MPa vertical stress. The initial conditions and selected states during testing are summarized in Tab. 2.

Tab. 2: Initial conditions and selected states during strain-controlled oedometer tests of Malaysian Kaolin with varying initial void ratios

Sample	No. 4	No. 5	No. 6
$\rho_{d,0}$ [g/cm^3]	1.24	1.35	1.44
w_0 [%]	15.8	15.3	14.8
e_0 [-]	1.18	1.00	0.88
S_{r0} [-]	0.36	0.41	0.45
$S_{r,final}$ [-]	0.75	0.72	0.71
e_{final} [-]	0.57	0.57	0.57
σ_{pre} [kPa]	560	900	1000
C_C [-]	0.53	0.54	0.53
C_S [-] (0.4 to 2 MPa)	0.04	0.06	0.07

A strain rate-controlled oedometer [9] was used. Fig. 5 shows the oedometer curves of the Malaysian kaolin with varying initial dry densities between 1.24, 1.35, and 1.44 g/cm^3, corresponding to void ratios of 1.18, 1.00 and 0.88, for samples 4, 5, and 6, respectively.

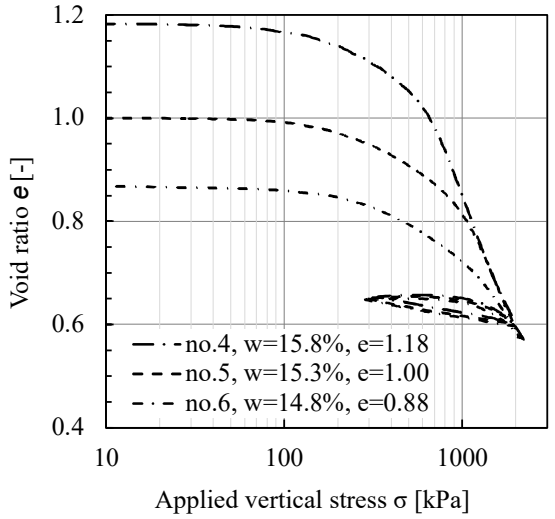

Fig. 5. Oedometer curves at similar initial water contents and varying initial void ratios

It can be seen that sample no. 4 (e = 1.18) shows normally consolidated behaviour from a vertical stress of approximately 560 kPa onwards. The preconsolidation stress of sample no. 4 is induced by the prior applied static compaction stress to the target void ratio of 1.18. Further, it is affected by the initial water content. Comparing with the compression curve of sample no. 1 having a comparable initial water content reveals that the compression line of sample no. 1 intersects at about 570 kPa with the void ratio value of 1.18, which is close to the above determined preconsolidation stress of 560 kPa for sample no. 4. The apparent preconsolidation stresses for samples 4, 5, and 6 were determined to be 560 kPa, 900 kPa and 1000 kPa, respectively, using the Casagrande's graphical method. The preconsolidation stress is affected by two inverse effects: a higher initial dry density results in higher prior compaction stress, and thus, higher preconsolidation stress. Contrary, a higher degree of saturation (smaller suction) leads to a smaller apparent preconsolidation stress. These two competing effects contribute to the preconsolidation stresses of the three samples. They are the reason why the obtained preconsolidation stress is

not directly proportional to neither dry density nor degree of saturation.

Furthermore, after hitting the normal consolidation line (NCL) the samples have similar compressibility. Thus, the compression indices C_C of samples no. 4, 5 and 6 are 0.53, 0.54 and 0.53, respectively. During unloading-reloading, the three samples exhibit a very similar behaviour. The corresponding swelling indices C_S of the samples no. 4, 5 and 6 are 0.04, 0.06 and 0.07, respectively.

4 Pore size distribution

In order to investigate the pore-size distribution (PSD) of the Malaysian kaolin and the influence of the water content on it, Mercury Intrusion Porosimetry (MIP) tests were performed on statically compacted samples having the same initial dry density corresponding to Proctor density, but varying water content. Three samples at a dry density of 1.35 g/cm^3 with water contents of w = 25%, w = 32%, and w = 35%, corresponding to the dry side, optimum, and the wet side, respectively, were compacted. After compaction, the samples were subjected to a freeze-drying procedure in order to remove the water without affecting the existing microstructure of the kaolin samples. The test results are presented as cumulative plot showing total intruded void ratio over pressure (Fig. 6) and differential volume over pore diameter (Fig. *7*).

The results of Fig. 6 indicate an existing discrepancy between the target compaction void ratio of 1.00 and the measured total intruded void ratio by MIP of 0.81 (for w = 25%), 0.79 (for w = 32%), and 0.70 (for w = 35%). This difference can be the result of disturbance during sample preparation or during pressurizing the sample in the MIP-device [10], where large pores greater than 400 µm can be compressed at the beginning of the pressure increase before the first mercury enters the pore space, leading to a reduced measured intruded pore volume as compared to the compacted state [12, 13].

Possible existing non-intrudable pores in the material has been often observed in case of bentonites for pore sizes smaller than 7 to 10 nm, depending on the maximum intrusion pressure of the device, and is usually not observed in case of non-active kaolin clays.

The density functions of the pore size distributions are shown in Fig. 7. The sample compacted at the dry side of optimum (Fig. 7a) shows a bi-modal pore-size distribution with peaks at pore sizes of 812 nm and 2221 nm, while the samples compacted at optimum water content (Fig. 7b) and at wet side of optimum (Fig. 7c) exhibit a mono-modal pore-size distribution with peaks at approximately 650 nm pore diameter. The results are in accordance to literature, e.g. [13, 14, 15], where samples compacted at the dry side were found to show a bi-modal pore size distribution, whereas samples compacted at the optimum water content and at the wet side exhibit a mono-modal pore-size distribution.

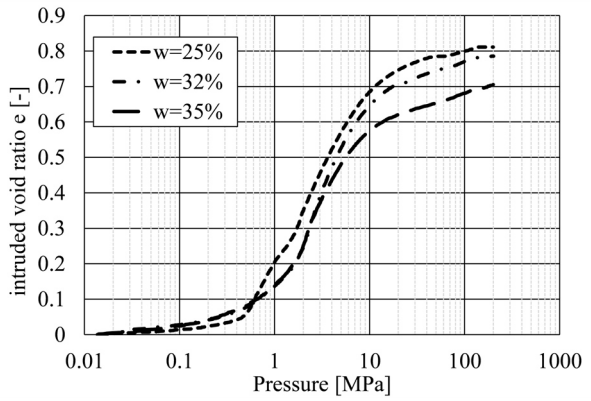

Fig. 6. Cumulative intruded pore volume of the three samples with initial void ratio e = 1.00

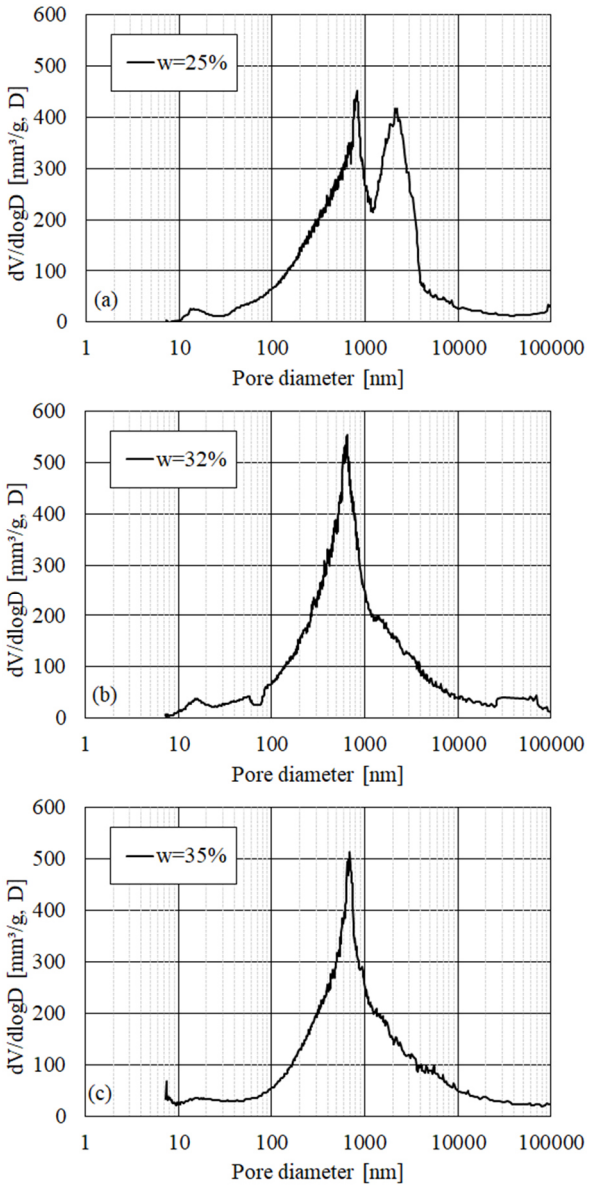

Fig. 7. Density functions of the compacted samples at void ratio e = 1.00 and **(a)** w = 25%, **(b)** w = 32%, **(c)** w = 35%

5 Soil Water Characteristic Curve

The drying Soil Water Characteristic Curves (drying SWCCs) were determined by means of the Vapour Equilibrium Technique (VET) and a Chilled Mirror

Hygrometer (CMH) according to [16] for two different initial material conditions. By this method, multiple samples prepared at identical initial conditions were subjected to drying in a desiccator at a high suction value of about 230 MPa. During the drying process, the samples were regularly weighted to determine the actual water content. The corresponding actual total suction was measured by means of the CMH and the Kelvin`s equation. Duplicate samples were used to measure the volume of the sample at given time steps. Fig. 8 shows the SWCC for a slurry (initial water content $w = 1.1\ w_L$) and for the initially unsaturated compacted sample (w = 32%, $\rho_d = 1.35$ g/cm³). Both SWCC data sets were fitted using the van Genuchten (vG) [17] equation (see eq. (1)).

$$S_r = \frac{S_{r,sat} - S_{r,res}}{(1+(\alpha*\psi)^n)^m} + S_{r,res} \quad (1)$$

The Air Entry Values (AEV) were determined as the inverse of the fitting parameter α [17, 18]. The fitting parameter α for the slurry was found to be 0.77 and for the compacted material it was 0.79, leading to very similar air-entry values of 1.29 MPa and 1.27 MPa, respectively. Tab. 3 summarizes the parameters determined with the least squares method. From Fig. 8 it can be seen that both materials are in the residual zone from approximately 10 MPa onwards.

Tab. 3: Fitting parameters for the drying SWCC according to van Genuchten [17] for initially compacted and slurry samples of Malaysian Kaolin

	Initially compacted	Slurry
α [-]	0.79	0.77
n [-]	2.42	3.17
m [-]	0.59	0.69
AEV [MPa]	1.27	1.29

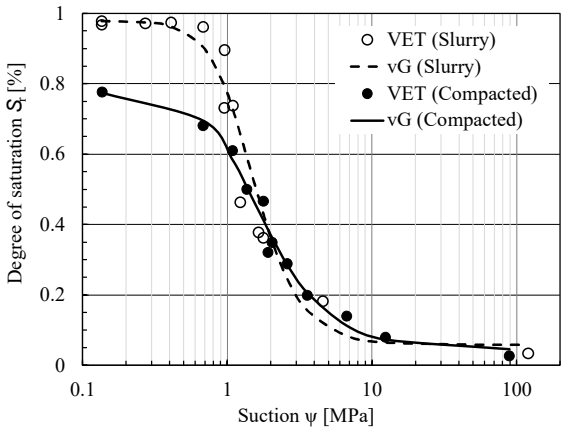

Fig. 8. Experimental data and SWCC determined on a slurry and a compacted sample of Malaysian Kaolin

6 Conclusion

Within the scope of this study, a thorough geotechnical characterisation of the Malaysian Kaolin was performed, including measurements of grain size distribution, plasticity properties and standard Proctor compaction curve.

In two different test series of strain-controlled oedometer tests, the effect of initial compaction conditions was investigated. While the determined preconsolidation stresses for samples with similar low initial dry density and varying initial water contents (series 1) are mainly controlled by the degree of saturation, thus suction, the preconsolidation stresses for the samples compacted at similar water content at dry side of optimum with varying initial dry densities (series 2) are controlled by the competing effects of both density and degree of saturation or suction. The compression index values of series 1 (C_C = 0.54 to 0.61) are slightly greater than those of series 2 (C_C = 0.53 to 0.54). At stresses greater than 4.5 MPa and 9.5 MPa, the NCLs merge in a single path, showing compression indices of 0.40 to 0.41. The swelling index values C_S of series 1 for a stress range between 1 and 10 MPa were found to be 0.08 to 0.09, thus, greater than those of test series 2 with C_S of 0.04 to 0.07, due to the greater stress, at which unloading was started.

The influence of water content on the microstructure of the material was determined by analysing MIP data. The water content at compaction plays a key role for the resulting pore-size distribution, which shows bi-modal shape for samples compacted at dry side of optimum, while samples compacted at optimum or at wet side of optimum exhibit a mono-modal pore-size distribution.

The drying soil water characteristic curves of a slurry sample and a compacted unsaturated sample were determined. The drying paths of two samples states join each other at suction of about 2 MPa. Further, the air-entry values of the slurry and the initially compacted sample are 1.29 and 1.27 MPa, thus, are very similar to each other.

Further experiments in the context of hydro-mechanical and thermo-hydromechanical behaviour of this material aiming its geothermal use in geotechnical structures are being currently performed.

Acknowledgements

The presented study has been performed within the project "Experimental and numerical investigation of coupled thermo-hydro-mechanical behaviour of clay with focus to cyclic processes" funded by the German Research Council (DFG, project No. WI 3180/11-1).

The authors are grateful to DFG for the financial support.

References

1. J.K.M. Gan, D.G. Fredlund, H. Rahadjo, Can. Geot. J. 25, 500-510 (1988)
2. J. Duque, Contributions to the experimental investigation and numerical description of soil cyclic behavior, Ph.D. Thesis, Charles University Prague, 25 pp (2021)

3. DIN EN ISO 17892-4, Geotechnical investigation and testing- Laboratory testing of soil- Part 4: Determination of particle size distribution (ISO 17892-4:2016); German version EN ISO 17892-4:2016, Beuth Verlag GmbH (2017)
4. DIN EN ISO 17892-12, Geotechnical investigation and testing- Laboratory testing of soil- Part 12: Determination of liquid limit and plastic limits (ISO 17892-12:2018); German version EN ISO 17892-12:2018, Beuth Verlag GmbH (2020)
5. J. Duque, M. Ochmański, D. Mašín, Y. Hong, L. Wang, Comput. Geotech. 134 (2021)
6. DIN 18196, Earthworks and foundations- Soil classification for civil engineering purposes, Beuth Verlag GmbH (2022)
7. DIN EN ISO 17892-3, Geotechnical investigation and testing- Laboratory testing of soil- Part 3: Determination of particle density (ISO 17892-3:2015, Corrected version 2015-12-15); German version EN ISO 17892-3:2015, Beuth Verlag GmbH (2016)
8. DIN 18127, Soil, investigation and testing – Proctor-test, Beuth Verlag GmbH (2012)
9. N. Müthing, On the consolidation behavior of fine-grained soils under cyclic loading, Ph.D. Thesis, Ruhr-Universität Bochum (2017)
10. D. Penumadu, J. Dean, Can. Geot. J. 37, 393–405 (2000)
11. W. Baille, S. Tripathy, T. Schanz, Appl. Clay Sci., 48(3):324–333 (2010) doi: 10.1016/j.clay.2010.01.002.
12. E. Romero, P. Simms, Geotech. Geol. Eng. 26, 705-727 (2008)
13. A. Tarantino, *Unsaturated soils: compacted versus reconstituted states*, in Proceedings of the 5th International Conference on Unsaturated Soils, 6-8 September 2010, Barcelona, Spain (2010)
14. L. Barden, G. Sides, J. Soil Mech. Found. Div., ASCE 96 (SM4), 1171–1200 (1970)
15. A. Sridharan, A. Altschaeffl, S. Diamond, J. Soil Mech. Found. Div., ASCE 97(SM5), 771–787 (1971)
16. A. Seiphoori, A. Ferrari, L. Laloui, Géotechnique 64, 721-734 (2014)
17. M.T. van Genuchten, Soil Sci. Soc. Am. J. 44, 892-898 (1980)
18. W. Baille, S. Tripathy, T. Schanz, VZJ, 13(5), doi: 10.2136/vzj2013.06.0112.